Martin, M. L., Delpuech, J.-J., & Martin, G. J. (1980) *Practical NMR Spectroscopy*, Heyden & Son, London.
McConnell, H. M. (1958) *J. Chem. Phys. 28*, 430–431.
Mildvan, A. S., & Gupta, R. K. (1978) *Methods Enzymol. 49*, 322–359.
Morris, A. T., & Dwek, R. A. (1977) *Q. Rev. Biophys. 10*, 421.
Nagahisa, A., Foo, T., Gut, M., & Orme-Johnson, W. H. (1985) *J. Biol. Chem. 260*, 846–851.
Omura, T., & Sato, R. (1964) *J. Biol. Chem. 239*, 2379–2385.
Orme-Johnson, N. R., Light, D. R., White-Stevens, R. W., & Orme-Johnson, W. H. (1979) *J. Biol. Chem. 254*, 2103–2111.
Philson, S. B., Debrunner, P. G., Schmidt, P. G., & Gunsalus, I. C. (1979) *J. Biol. Chem. 254*, 10173–10179.
Poulos, T. L., Finzel, B. C., Gunsalus, I. C., Wagner, G. C., & Kraut, J. (1985) *J. Biol. Chem. 260*, 16122–16130.
Poulos, T. L., Finzel, B. C., & Howard, A. J. (1986) *Biochemistry 25*, 5314–5322.
Rein, H., Maricic, S., Janig, G.-R., Vuk-Pavlovic, S., Benko, B., Ristau, O., & Ruckpaul, K. (1976) *Biochim. Biophys. Acta 446*, 325–330.
Sheets, J. J., & Vickery, L. E. (1982) *Proc. Natl. Acad. Sci. U.S.A. 79*, 5773–5777.
Sheets, J. J., & Vickery, L. E. (1983) *J. Biol. Chem. 258*, 1720–1725.
Simpson, E. R. (1979) *Mol. Cell. Endocrinol. 13*, 213–227.
Solomon, I. (1951) *Phys. Rev. 99*, 559–565.
Solomon, I., & Bloembergen, N. (1956) *J. Phys. Chem. 25*, 261–266.
Vickery, L. E., & Kellis, J. T. (1983) *J. Biol. Chem. 258*, 3832–3836.
White, R. E., & Coon, M. J. (1980) *Annu. Rev. Biochem. 49*, 315–356.

Characterization of Interaction between DNA and 4′,6-Diamidino-2-phenylindole by Optical Spectroscopy†

Mikael Kubista, Björn Åkerman, and Bengt Nordén*
Department of Physical Chemistry, Chalmers University of Technology, S-41296 Göteborg, Sweden
Received October 2, 1986; Revised Manuscript Received February 18, 1987

ABSTRACT: We have examined the interaction between 4′,6-diamidino-2-phenylindole (DAPI) and DNA using flow linear dichroism (LD), circular dichroism (CD), and fluorescence techniques. We show the presence of two spectroscopically distinct binding sites at low binding ratios with saturation values of 0.025 and 0.17, respectively. In both sites DAPI is bound with its long axis approximately parallel to the grooves of the DNA helix. Resolution of CD spectra shows that an exciton component is present at higher binding ratios, which we attribute to the interaction of two accidentally close-lying DAPI molecules. We also find evidence that DAPI, at least in the high-affinity site, binds preferentially to AT-rich regions. From the spectroscopic results, supported by structural considerations, we can completely exclude that DAPI is bound to DNA by intercalation. Binding geometries and site densities are consistent with a location of DAPI in the grooves of DNA, with the high-affinity site most probably in the minor groove.

The trypanocide 4′,6-diamidino-2-phenylindole (DAPI),[1] first

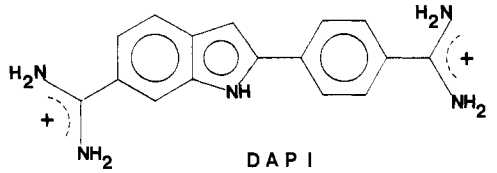

DAPI

synthesized by Dann et al. (1971), has been shown to bind reversibly to DNA as evidenced by fluorescence enhancement and sedimentation experiments in cytochemical studies (Williamson & Fennel, 1975) and by changes in absorption (Lin et al., 1977; Chandra & Mildner, 1979) and fluorescence spectra (Lin et al., 1977). A large increase in the fluorescence quantum yield of DAPI upon binding to nucleic acids has been reported (Williamson & Fennel, 1975; Kapuscinski & Skoczyklas, 1978). The increase seems to be specific for double-stranded DNA and has not been observed together with RNA or single-stranded DNA [poly(rI) being the only exception] (Kapuscinski & Szer, 1979), and it seems to be largest in AT-rich regions (Williamson & Fennel, 1975; Schweizer, 1976; Lin et al., 1977; Kapuscinski & Szer, 1979; Cavatorta et al., 1985). These properties have made DAPI very useful in cytochemical investigations (Williamson & Fennel, 1975; Schweizer, 1976; Langlois et al., 1980; Coleman et al., 1981; Tijssen et al., 1982; Lee et al., 1984), as a marker in DNA electrophoresis (Kapuscinski & Yanagi, 1979; Naimski et al., 1980), and in DNA–protein interaction studies (Kania & Fanning, 1976; Stepien et al., 1979; Mazus et al., 1986). DAPI has also been used in protein investigations, e.g., with tubulin (Bonnet et al., 1985).

Recent circular dichroism (CD) measurements show that DAPI binds to DNA in two spectroscopically distinct sites.

†This project is supported by The Swedish Natural Science Research Council and The National Swedish Board for Technical Development.
*Author to whom correspondence should be addressed.

[1] Abbreviations: DAPI, 4′,6-diamidino-2-phenylindole; LD, linear dichroism; CD, circular dichroism; LD′, reduced linear dichroism; A_{iso}, isotropic absorbance; EDTA, ethylenediaminetetraacetic acid; R, ratio of total amount of DAPI to DNA phosphate; r, ratio of bound DAPI to DNA phosphate; $\Delta\epsilon$, difference in molar absorptivity between left- and right-handed circularly polarized light.

0006-2960/87/0426-4545$01.50/0

These are present independently of base content and sequence and have slightly different binding characteristics. The binding constant for the site with the higher affinity is shown to increase with increasing content of AT clusters (Manzini et al., 1983). This is in agreement with earlier reports of DAPI binding preferentially to AT-rich regions (Kapuscinski & Skoczyklas, 1977; Chandra & Mildner, 1979; Masotti et al., 1982). The existence of two binding sites with high affinity has also been suggested on the basis of fluorescence measurements. These are characterized by a large increase in the fluorescence quantum yield and are suggested to be situated in AT-rich regions (Kapuscinski & Skoczylas, 1978; Kapuscinski & Szer, 1979). However, the binding characteristics (binding constants and saturation values) in these studies are different. The saturation values from the fluorescence study are lower than those obtained with CD and, the authors speculate, in an additional nonfluorescent weak type of binding without any base specificity. Some of the differences may probably be ascribed to the different salt concentrations used in the studies. Using CD, Manzini et al. (1983) have shown that binding in both modes is highly sensitive to the ionic strength: the binding constant for the weaker site, and to a lesser extent for the stronger one, decreases with increasing ionic strength. The authors ascribe this salt dependence to an electrostatic component in the mode of binding. An additional mode of interaction has been proposed on the basis of altered characteristics in the fluorescence spectrum at high dye/phosphate ratios and has been suggested to correspond to a binding of additional DAPI in the proximity of previously bound molecules (Cavatorta et al., 1985).

The nature of the mode of interaction of DAPI with DNA is far from fully understood. Intercalation, at low as well as high binding ratios, has been suggested on the basis of calorimetric (Chandra & Mildner, 1979) and solvent effect studies (Masotti et al., 1982), from the stabilization toward thermal denaturation and on the similarity, in some aspects, with the behavior of known intercalators (Kapuscinski & Skoczylas, 1978; Masotti et al., 1982). However, there are also strong arguments against intercalative binding: measurements in a large range of binding ratios of the unwinding of supercoiled DNA induced by DAPI (Stepien et al., 1979; Manzini et al., 1983) and the sedimentation of linear DNA with bound DAPI (Ford & Rickwood, 1984) do not show the characteristic behavior of intercalating ligands (Waring, 1970; Ford & Rickwood, 1984). DAPI behaves in these studies more like netropsin, which is established as a nonintercalator (Patel, 1982; Dattagupta et al., 1980). The conclusiveness of the unwinding experiments has been questioned (Kapuscinski & Skoczylas, 1978), because of the absence of lateral substituents in DAPI (contrary to, e.g., ethidium) that might result in a low unwinding angle comparable to that of proflavin (which is known to intercalate). However, recent measurements have shown a distinctly different behavior of DAPI compared to proflavin in unwinding and sedimentation experiments (Manzini et al., 1983; Ford & Rickwood, 1984).

Speculations on the structure of the DAPI–DNA complex have been made on the basis of comparison with other nonintercalators. The resemblance from several angles with netropsin, which is evidenced to bind in the minor groove of DNA (Dattagupta et al., 1980; Patel, 1982), has led to the proposal that the high-affinity site is located in the minor groove, with DAPI forming hydrogen bonds with the DNA bases and with an electrostatic attraction between the amidino groups of DAPI and the DNA phosphates (Manzini et al., 1984). This hypothesis is in accordance with affinity chromatography experiments (Chandra & Mildner, 1979) and with the estimated site size obtained from molecular models (Manzini et al., 1983). Structural information from spectroscopic measurements has so far been limited because of the relatively unknown electronic structure of the DAPI molecule, and more work is needed to fully understand the interaction of DAPI with DNA.

In this study we use flow linear dichroism (LD) spectroscopy to determine the average angle between the long axis of DAPI and the DNA helix axis. We repeat the CD measurements of Manzini et al. (1983) and can confirm the existence of two sites at intermediate binding ratios, but we also find new, more conclusive indications for an additional mode of interaction at high dye/phosphate ratios. The absorption, CD and LD, spectra are resolved into site-specific contributions. On the basis of the knowledge that the corresponding transition moments are directed essentially along the molecular long axis of DAPI (B. Åkerman, M. Kubista, and B. Nordén, unpublished results), the results are interpreted in terms of structural parameters and conclusions about the location of DAPI in the two sites.

Materials and Methods

Chemicals. All chemicals used were of analytical grade, and aqueous solutions were prepared with deionized and triply filtered water (Millipore). Calf thymus DNA was purchased from Sigma (type I) and DAPI from Serva, both used without further purification. All measurements were performed in 10 mM NaCl/0.1 mM EDTA solution, if not otherwise stated, and at room temperature. The pH was checked regularly and was always between 6.7 and 7.0.

Concentrations of stock solutions were determined spectrophotometrically, with the molar extinction coefficients of 6600 (260 nm) and 27 000 (340 nm) M^{-1} cm^{-1} for DNA (Mahler et al., 1964) and DAPI (Kapuscinski & Skoczylas, 1978), respectively. Measurement series, covering a comprehensive range of DAPI/DNA ratios (R, defined as the ratio of total amount of DAPI to DNA phosphate), were performed at either constant DNA or constant DAPI concentration. The concentration of a component was kept constant by mixing solutions with identical concentrations with respect to the component.

Linear Dichroism Spectroscopy. LD at a given wavelength is defined as

$$LD = A_{\parallel} - A_{\perp} \quad (1)$$

where $A_{\parallel}$ and $A_{\perp}$ are the absorbances of linearly polarized light, with the direction of polarization, parallel and perpendicular, respectively, to a macroscopic orientation direction. The reduced dichroism LD^r, was calculated as

$$LD^r = LD/A_{iso} \quad (2)$$

with A_{iso} the absorbance of the same isotropic sample (at rest).

LD spectra were measured on a Jasco J-500 spectropolarimeter, with an achromatic quarter wave device installed in the incoming light beam converting the polarizations of light from circular into linear as described elsewhere (Davidsson & Nordén, 1976). An absolute correctness of the LD measurement was ascertained in the whole wavelength region according to a calibration method described elsewhere (Nordén & Seth, 1985). The DNA samples were oriented in a Couette cell, as designed by Wada and Kozawa (1964) and described by Nordén and Tjerneld (1976). A_{iso} was measured on a Cary 219 spectrophotometer, whose monochromator was wavelength-matched with the Jasco instrument.

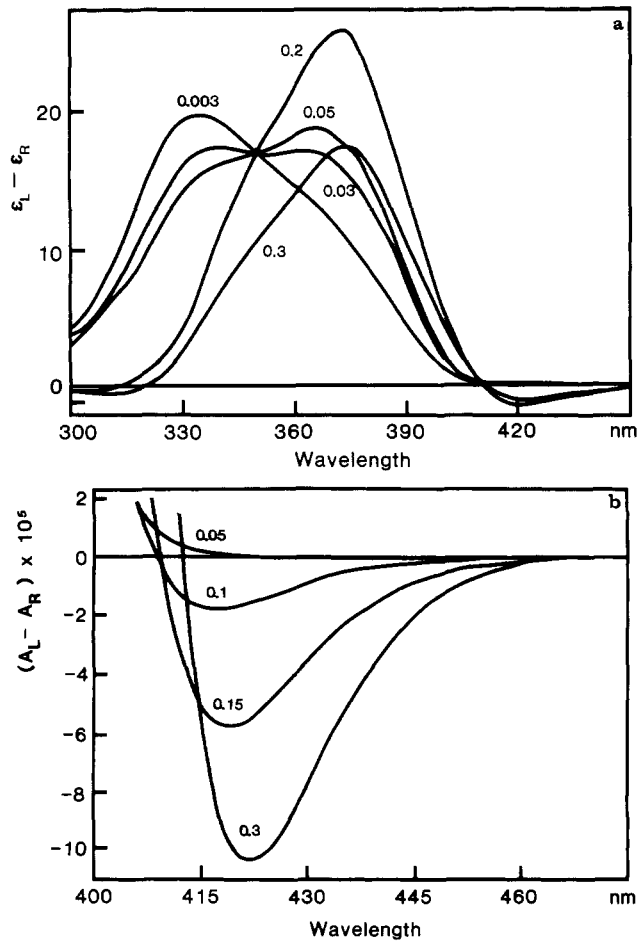

FIGURE 1: CD spectra of DAPI–DNA complexes at different dye/phosphate ratios (indicated in the figure): (a) spectra normalized to unit DAPI concentration; (b) the region 400–475 nm at constant DNA concentration (0.33×10^{-3} M) normalized to 1-cm optical path length.

The angle between the light-absorbing transition moment and the DNA helix axis is related to the corresponding LD^r according to (Matsouka & Nordén, 1982, 1983)

$$LD^r = 3S(3\langle\cos^2\alpha\rangle - 1)/2 \qquad (3)$$

where $\langle\alpha\rangle$ denotes an ensemble average and S is an orientation factor in the range 0–1 and depends on the degree of orientation. The orientation factor was determined from the DNA base absorption at 260 nm with an apparent angle of 86° (Arnott et al., 1969; Matsuoka & Nordén, 1982, 1983). The orientating flow gradient was in all experiments $1800 \pm 2\ s^{-1}$.

Absorption and Circular Dichroism Spectroscopy. Absorption spectra were measured on the Cary spectrophotometer, with cell widths ranging from 0.1 to 1 cm. CD spectra were measured correspondingly on the Jasco instrument.

Fluorescence Spectroscopy. Fluorescence measurements were performed on an AMINCO SPF-500 "corrected spectra" spectrofluorometer. To avoid changes in the fluorescence intensity due to internal motion, the isotropic fluorescence was measured with a vertically oriented excitation polarizer and with the emission polarizer set at the "magic angle" of 54.7° to the vertical direction. The fluorescence measured in this way will be referred to as the F_{55}-fluorescence.

RESULTS

Figure 1a shows CD spectra of DAPI–DNA complexes at different R normalized with respect to DAPI concentration. At very low ratios, a CD maximum is observed at 335 nm with a shoulder at ~365 nm. At increasing ratios the CD signal decreases at shorter wavelengths with a concomitant increase of the shoulder and becomes approximately "reversed" at $R = 0.05$ with a shoulder at 340 nm and a peak at 375 nm. Up to $R \sim 0.2$, the CD signal remains constant at 351 nm, indicating the presence of an isodichroic point with a $\Delta\epsilon$ ($=\epsilon_L - \epsilon_R$) of 17 $M^{-1}\ cm^{-1}$. At $R > 0.05$ additional negative CD components are observed to develop below 320 nm as well as above 400 nm. Figure 1b shows the 400–460-nm region normalized to constant DNA concentration. The negative CD signal in this region is observed to increase in a nonlinear manner with R, and subsequent CD curves intersect each other at increasing wavelengths.

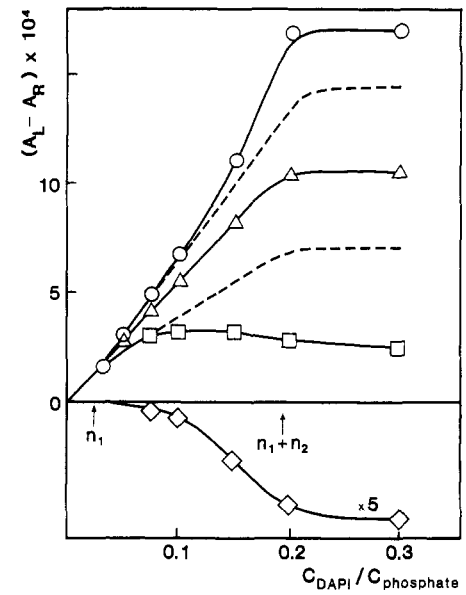

FIGURE 2: CD signal as a function of DAPI/DNA ratio: CD at 350 (△), 371 (○), 330 (□), and 422 nm (◇); DNA concentration 0.33 $\times 10^{-3}$ M; optical path 1 cm. Determined values of n_1 (by eq 15) and $n_1 + n_2$ (from extrapolation of the initial slope of the CD signal at 351 nm to the saturation plateau) are indicated in the figure. Dashed curves represent CD signals corrected for dimer exciton contribution (see text).

Figure 2 shows the CD signal at a few selected wavelengths plotted vs. R. Except at 422 nm, all CD signals increase initially linearly with R and approach saturation approximately at $R = 0.2$. At 422 nm a negative CD is observed above $R = 0.05$ that increases sigmoidally with R.

Figure 3 shows LD, A_{iso}, and LD^r spectra for DAPI–DNA complexes at $R = 0.01$ and $R = 0.05$. The LD in the absorbing region of the DNA bases, 240–280 nm, is negative as expected for double-stranded DNA with the planes of the bases oriented more or less perpendicularly to the DNA helix. The LD for the DAPI absorption, 300–400 nm, is positive, demonstrating that DAPI is oriented more parallel than perpendicular to the DNA axis, a geometry that excludes true intercalation. The normalized isotropic absorbance of DAPI is significantly lower at $R = 0.05$ than at $R = 0.01$ (note that the scale factors in Figure 2 are chosen to compensate for the difference in the DAPI concentration between the two samples), but the absorption profiles are, within experimental error, identical in shape. A corresponding decrease in extinction coefficient with increasing binding ratio has been reported for several other DNA binding chromophores (Müller & Gautier, 1975). The amount of bound DAPI was therefore more accurately determined from the CD signal at the isodichroic point at 351 nm than from absorption measurement.

The LD^r of the DNA bases is at $R = 0.01$ almost independent of wavelength, as expected for the B-form DNA configuration (Matsuoka & Nordén, 1982, 1983). At $R =$

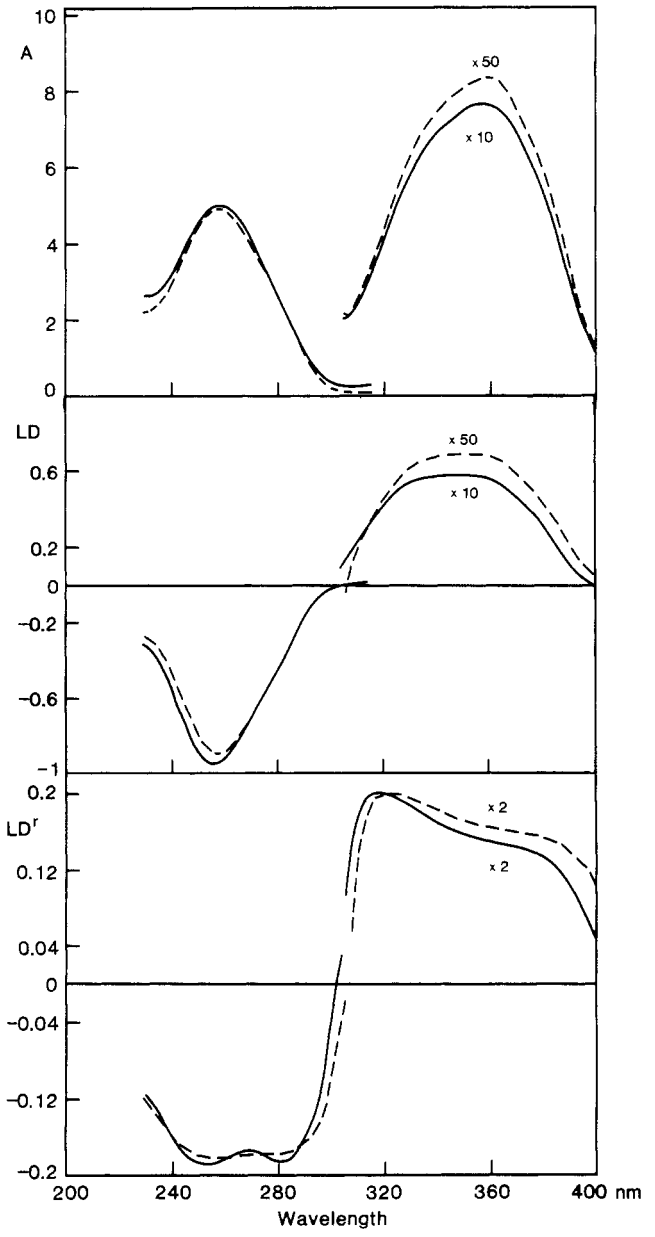

FIGURE 3: Absorbance (A), linear dichroism (LD), and reduced linear dichroism (LD^r) spectra of DAPI–DNA complexes at $R = 0.01$ (---) and $R = 0.05$ (—). DNA concentration 0.72×10^{-3} and optical path 1 cm.

0.05, a small wavelength dependence is observed that is most probably due to the absorption band of DAPI at 260 nm (Kapusciski & Skoczyklas, 1978). The overall amplitude of the LD^r in this region is practically the same at both ratios, suggesting approximately the same degree of DNA orientation. The LD^r of the DAPI absorption is postitive and decreases somewhat at longer wavelengths. The signal at $R = 0.05$ is reduced by some 10%, compared to $R = 0.01$, and the wavelength dependence is slightly more pronounced.

Figure 4 shows the F_{55}-fluorescence intensity of DAPI as a function of R. The same instrumental conditions were maintained throughout the measurements, and the DAPI concentration was held constant with high accuracy (±2%). The intensity increases continuously with decreasing R, and not even at $R = 10^{-4}$ was any saturation observed.

Discussion

Interaction between DAPI and DNA. DAPI has been proposed to have at least two different binding sites in DNA (Kapuscinski & Skoczylas, 1978; Manzini et al., 1983; Cavatorta et al., 1985). The distinct changes in the CD spectrum during titration (Figure 1a), the accompanying decrease of the normalized absorbance, and the variation of LD and LD^r spectra between $R = 0.01$ and $R = 0.05$ (Figure 3) all suggest that the average characteristics of bound DAPI are markedly changed between these two binding ratios. Still the emission profile remains essentially unchanged between these ratios, nor does it change with excitation wavelength (results not shown). This is not in conflict with the hypothesis of more than one binding site since the absorption profile too is constant between $R = 0.01$ and $R = 0.05$ (Figure 3), showing that the absorption spectrum of DAPI in these sites has the same shape.

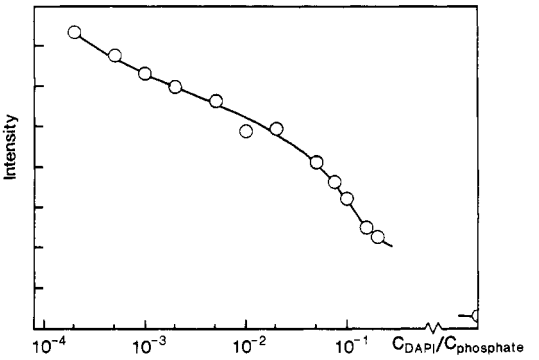

FIGURE 4: F_{55}-fluorescence intensity as a function of DAPI/DNA ratio at a constant DAPI concentration of 0.05×10^{-6} M: excitation wavelength 360 nm and emission wavelength 450 nm (slit width 4 and 10 nm for excitation and emission, respectively, arbitrary intensity scale).

The occurrence of an isodichroic point at 351 nm for $R < 0.3$ (Figure 1a; Manzini et al., 1983) indicates that there are precisely two distinct CD active species in this range of binding ratios. On the basis of this hypothesis we shall resolve CD, LD, and absorbance spectra into contributions specific for the two DAPI–DNA complexes.

Resolution of CD Spectra. The drastic changes in the CD spectrum during titration (Figure 1a) are hard to explain with only one transition in the visible region of DAPI, because the CD spectrum of a single transition can be anticipated to have the same shape as its corresponding absorption envelope (Cantor & Schimmel, 1980). We shall assume that there are two transitions in this region, corresponding to different optical activity in the two sites. This hypothesis is supported by the wavelength dependence in the LD^r spectrum (Figure 3) and by recent measurements on DAPI oriented in stretched films (B. Åkerman, M. Kubista, and B. Nordén, unpublished results). By taking a CD spectrum at a certain binding ratio and subtracting from it the CD spectrum measured at some other ratio, times a weight factor that is tuned to give a vanishing CD for one of the two transitions, one will obtain the CD profile of the other transition. This is illustrated with $R = 0.08$ and $R = 0.003$ in Figure 5 and provides the profile of transition II, $T_{II}(\lambda)$. The profile of transition I, $T_I(\lambda)$, is obtained analogously.

The normalized CD spectra at low binding ratios ($R < 0.005$) were identical within experimental error and therefore were assumed to represent the pure spectrum of DAPI in site 1 (the binding site with the larger affinity). This spectrum was satisfactorily resolved into the two transition profiles, T_I and T_{II}, by using a nonlinear best fit analysis.

After the CD amplitude of the two transitions is normalized to unity in site 1, any CD spectrum below $R = 0.08$ (where the negative CD components are still absent) can be satisfactorily resolved into the two transitions:

$$CD(R,\lambda) = t_I(R)T_I(\lambda) + t_{II}(R)T_{II}(\lambda) \qquad (4)$$

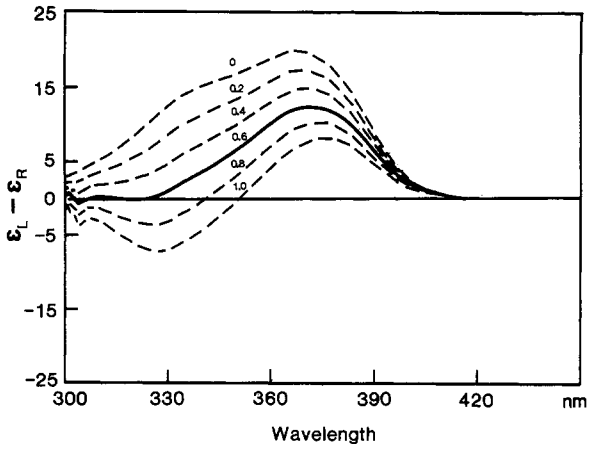

FIGURE 5: Linear combinations of two normalized CD spectra, CD(r = 0.08) − K × CD(r = 0.003); scale factors K indicated in figure. The profile obtained with K = 0.6 (—) was used for transition I in the resolution.

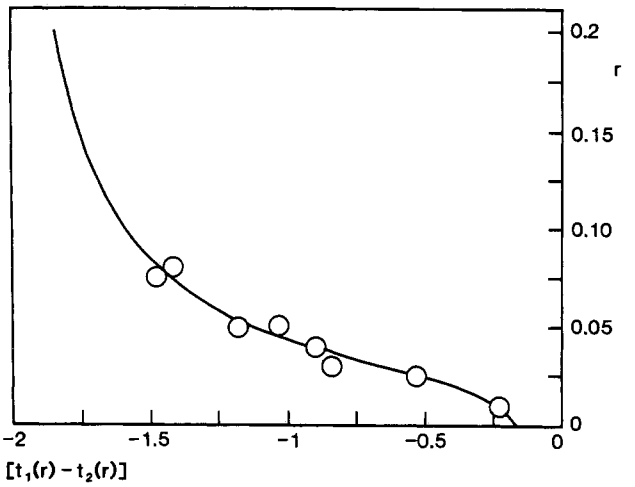

FIGURE 6: Best fit of eq 15 to experimental points. Difference between the proportions of the two transitions vs. binding ratio (see text).

where CD(R,λ) denotes a normalized CD spectrum at ratio R. T_I and T_{II} are the normalized profiles (relative to site 1) of the two transitions, and $t_I(R)$ and $t_{II}(R)$ are their respective contributions.

In order to find the CD spectrum for site 2, we first make use of the isodichroic point at 351 nm. As long as this is present, it is justified to assume that all DAPI molecules are bound to DNA (R can then be replaced by the true binding ratio r = $DAPI_{bound}/DNA_{phosphate}$), and the CD spectrum may be written as a linear combination of CD contributions from the two sites:

$$CD(r,\lambda) = f(r)CD_1(\lambda) + [1 - f(r)]CD_2(\lambda) \quad (5)$$

CD_1 and CD_2 are the CD spectra of DAPI in sites 1 and 2, respectively, and $f(r)$ is the fraction in site 1 at ratio r. The two "site-specific" spectra are in turn composed of components from the two transitions:

$$CD_1(\lambda) = T_I(\lambda) + T_{II}(\lambda) \quad (6)$$
$$CD_2(\lambda) = aT_I(\lambda) + bT_{II}(\lambda)$$

where a and b are constants to be determined.

At the isodichroic point, both sites contribute equally. This gives a relation between a and b:

$$(a - 1)/(b - 1) = -[T_{II}(351\text{ nm})/T_I(351\text{ nm})] = -0.42 \quad (7)$$

The second necessary relation between a and b will be obtained as follows. Assuming that the two sites are distinct, the following equilibria can be used:

$$K_i = [S_iL]/[S_i][L] \quad (8)$$

where K_i is the equilibrium constant for binding to site i (i = 1, 2) and $[S_iL]$, $[L]$, and $[S_i]$ are the concentrations of bound ligand in site i, free ligand, and unoccupied site i, respectively. Dividing K_1 by K_2, defining a "site partition constant" K, eliminates the unknown $[L]$ and gives

$$K = K_1/K_2 = ([S_1L][S_2])/([S_2L][S_1]) \quad (9)$$

Introducing total concentrations of sites and ligands $[S_i]_{tot}$ and $[L]_{tot}$ gives after rearrangement

$$K = \frac{[S_1L][S_2]_{tot} - [L]_{tot}[S_1L] + [S_1L]^2}{[S_1]_{tot}[L]_{tot} - ([L]_{tot} + [S_1]_{tot})[S_1L] + [S_1L]^2} \quad (10)$$

Dividing through by $[L]_{tot}^2$ and recalling that $[S_1L]/[L]_{tot}$ = $f(r)$ and $[S_i]_{tot}/[L]_{tot} = n_i[L]_{tot}/(r[L]_{tot}) = n_i/r$, where n_i is the fraction of binding sites i per nucleotide (the site density), gives

$$K = \frac{(n_2/r - 1)f(r) + f^2(r)}{n_1/r - (1 + n_1/r)f(r) + f^2(r)} \quad (11)$$

which may also be expressed in the fraction, $1 - f(r)$, bound to site 2:

$$K = \frac{n_2/r - (1 + n_2/r)[1 - f(r)] + [1 - f(r)]^2}{(n_1/r - 1)[1 - f(r)] + [1 - f(r)]^2} \quad (12)$$

An expression for $1 - f(r)$ is obtained by substitution of eq 5 into eq 6:

$$CD(r,\lambda) = [f(r) + a[1 - f(r)]]T_I(\lambda) + [f(r) + b[1 - f(r)]]T_{II}(\lambda) \quad (13)$$

Identification with eq 4 shows that the portions of the respective CD contributions can be expressed as

$$t_I(r) = f(r) + a[1 - f(r)] \quad (14)$$
$$t_{II}(r) = f(r) + b[1 - f(r)]$$

and the difference gives the necessary expression for $1 - f(r)$:

$$t_I(r) - t_{II}(r) = (a - b)[1 - f(r)]$$

The ratio $[t_I(r) - t_{II}(r)]/(a - b)$ is defined as A, and eq 12 is solved for r:

$$r = [A(n_1K + n_2) - n_2]/[(A^2 - A)(1 - K)] \quad (15)$$

The best fit of experimental data to eq 15 is shown in Figure 6 with $t_I(r) - t_{II}(r)$ as the abscissa and r as the ordinate. Only binding ratios where the negative CD components are absent (r < 0.08) have been used. The parameters obtained in eq 15 were (uncertainties in parentheses) n_1 = 0.025 (0.004); n_2 = 0.19 (0.04); $K = K_1/K_2$ = 90 (50); and $a - b$ = −2.12 (0.06). The fit was very sensitive to the values of n_1 and $a - b$ as shown by the estimated uncertainties. This second relation between a and b, together with eq 7, enables the evaluation of these constants and the determination of the specific spectrum for site 2. The site specific CD spectra, together with their respective transition components, are shown in Figure 7.

DAPI–DAPI Interactions. An additional component appears in the CD spectrum at binding ratios above 0.05 (Figure 1b). Since it is observed when the isodichroic point is still present (ratios between 0.08 and 0.2), we find it justified to assume that this CD is a contribution from DAPI molecules

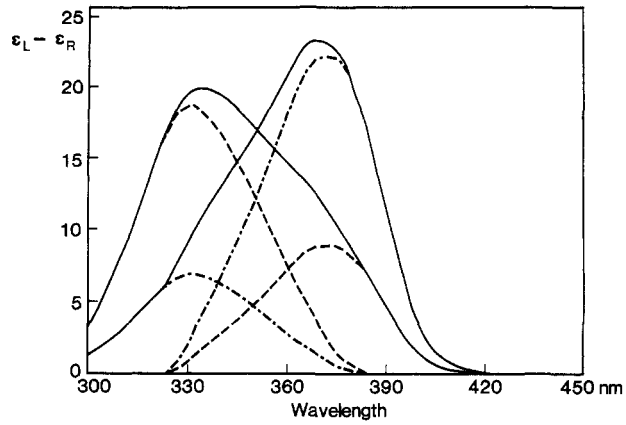

FIGURE 7: The two resolved site-specific CD spectra in turn resolved with respect to contributions from two transitions (T_I, T_{II}).

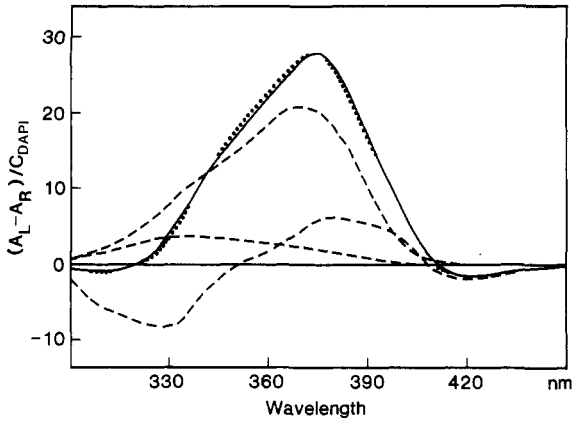

FIGURE 8: Experimental CD spectrum at $R = 0.3$ normalized to unit concentrations of bound DAPI (—). Reconstructed spectrum (···) from the two monomeric (site 1 and 2) and the dimer exciton contributions.

already bound in site 1 and/or site 2. The shape of this component is obtained by subtraction of appropriate amounts of the site-specific spectra by using eq 15. The result was found to be essentially independent of R. The two site-specific spectra together with this component can account for all the features in the CD spectra observed during titration (Figure 1a). This is further demonstrated in Figure 8, where the CD spectrum at $R = 0.3$ (the binding is then no longer quantitative) can be successfully resolved into these contributions.

There are several arguments indicating that the additional component in the CD spectrum *is not due to a third species* but arises from interactions between DAPI molecules in site 1 and/or site 2 bound in accidental proximity to each other: (a) the CD component appears at binding ratios where the isodichroic point is still present (cf. $R = 0.2$ in Figure 1a), (b) it increases sigmoidally in magnitude with R (Figure 2) as is expected for an "accidental dimer" (Gardner & Mason, 1967; Nordén & Tjerneld, 1982), (c) it cannot be related to the two transitions in the way expected for a monomeric, DNA-induced CD, (d) it has both positive and negative contributions as expected for exciton CD (two identical electric-dipole allowed transitions, chirally oriented relative to each other, exhibit exciton CD with one positive and one negative lobe of equal magnitudes).

The sign order of the lobes is determined by the geometry (the helicity) of the dimer (Cantor & Schimmel, 1980). The additional component has negative lobes at both short and long wavelengths and is positive in between. Since DAPI has two transitions, two exciton couplets are expected according to the degenerate exciton coupling. The sign order appears to be opposite for the two transitions, which can indicate that the two moments are arranged with opposite helicity. Such an arrangement is obtained, for example, if one of the monomers is "upside down" relative to the other. If one monomer is in site 1 and the other in site 2, this could also account for the apparent "mirror plane" at 350 nm of the two site-specific CD spectra (Figure 7), since transition I in site 1 would sense the environment of transition II in site 2 and vice versa.

DAPI–DAPI interaction is also evidenced from fluorescence measurements, where a broadening of the emission profile is observed at high binding ratios (results not shown; Cavatorta et al., 1985).

Binding Data. The binding data calculated above from the resolution of the CD spectra into site-specific components can also be related to the titration curves shown in Figure 2. The CD signal at 351 nm, which corresponds to the isodichroic point (Figure 1a) and where the dimer contribution is almost zero (Figure 8), increases initially linearly with R, indicating quantitative binding. The signal saturates at higher ratios, and the ratio, at the point where the extrapolated initial slope crosses the saturation level, is expected to be $n_1 + n_2$. The crossing point is observed at $R = 0.195$, which is well in accord with the estimated value of 0.21 ± 0.04 from the fit of eq 15 to experimental data. Because the uncertainty in the fitted value of n_2 is much larger than that of n_1, the most accurate value of n_2 from our measurements is $n_1 + n_2$ (from Figure 2) $- n_1$ (from eq 15), which yields $n_2 = 0.17$.

The CD signal at 371 and 330 nm increases approximately linearly for binding ratios less than 0.075. At higher ratios there is a curvature owing to the contribution from exciton CD. The exciton contribution is obtained from the CD signal at 422 nm (where monomeric CD is zero) and can be deducted by using an appropriate amount of the exciton spectrum in Figure 8. The CD contributions from noninteracting DAPI molecules are represented by the dashed curves in Figure 2. In the work of Manzini et al. (1983), these authors assume that only site 1 contributes to the CD signal at 335 nm. The signal at 330 nm is observed to reach a virtual "saturation level" (Figure 2); however, this is owing to a cancelling effect between a positive contribution from site 2 (Figure 7) and a negative contribution from the dimers (Figure 8). Extrapolation of the initial slope at 330 nm to this saturation level gives a crossing point at a ratio as high as ~0.07, explaining the significant difference between their saturation value of site 1 (0.06) and ours (0.025). The fact that the contribution from the exciton CD is almost zero at the isodichroic point at 351 nm (Figure 8) indicates that the value of the total saturation, $n_1 + n_2$, which Manzini et al. obtained from their Scatchard plot at this wavelength, should be essentially correct. We cannot fully explain the difference between their $n_1 + n_2$ value (0.29) and ours (0.20), but it can in part be ascribed to different extinction coefficients used in the determination of the DAPI concentration.

From the determined ratio, K_1/K_2, and the knowledge of K_1, being approximately 1×10^7 M^{-1} at the present ionic strength (Kapuscinski & Skoczylas, 1978; Manzini et al., 1983), one can estimate K_2 to be approximately 1×10^5 M^{-1}.

Preferential Binding to AT-Rich Regions. DAPI has been proposed to exhibit a binding preferentiality to AT-rich regions (Chandra & Mildner, 1979; Manzini et al., 1983). An AT preferentially *within site 1* is in fact supported by evidence from our fluorescence measurements. As seen in Figure 4, the F_{55}-fluorescence, as a function of R, shows a considerable decrease with increasing binding ratio, already in the region 10^{-4}–10^{-2} DAPI/DNA *where all DAPI is bound to site 1.* A

Table I: Spectroscopic Data for DAPI–DNA

	CD[a] (M^{-1} cm^{-1})					LD[c]	
site	$\Delta\epsilon_{351}$	$\Delta\epsilon_{331}$	$\Delta\epsilon_{373}$	$\Delta\epsilon_{max}$	A^b (M^{-1} cm^{-1}), ϵ_{359}	LD^r_{sw}	LD^r_{lw}
1	17.0	18.7	8.9	19.9 (335 nm)	22600	0.87 (43.5°)	0.66 (46.1°)
2	17.0	6.9	22.2	23.3 (369 nm)	18600	0.70 (45.6°)	0.46 (48.7°)

[a] Decadic circular dichroisms at the isodichroic point (351 nm), at the wavelengths of the maxima of transition I (331 nm) and transition II (373 nm), and at the maximum of the overall CD. [b] Molar absorptivity at the absorption maximum (359 nm). [c] LD^r values for the two transitions estimated at their short- and long-wavelength wings in Figure 9 (sw and lw). Calculated apparent angles by means of eq 3 are given in parentheses. The uncertainties in the LD^r values are estimated to ±0.05, corresponding to approximately ±1° in these angles.

corresponding study with poly(dA-dT) shows no decrease at all in this region (results not shown). This indicates a heterogeneity within site 1, and on the basis of the higher fluorescence quantum yield observed for DAPI bound to AT-rich DNA (Kapuscinski & Szer, 1979; Cavatorta et al., 1985), we conclude that this effect is owing to a preferential binding of DAPI within site 1 to AT-rich DNA segments. (A corresponding preferentiality is probable also in site 2 as in fact suggested by the fluorescence behavior at higher binding ratios.) Note that there is no saturation of the F_{55} intensity in Figure 4 with decreasing binding ratio. This is not unexpected for statistical reasons owing to the sparse occurrence of long, pure AT segments in DNA and the low binding density of site 1.

Our interpretation is in agreement with a reported increase of the binding constant for site 1 with increasing content of AT clusters (Manzini et al., 1983). Further, a binding study based on fluorescence yielded nonlinear Scatchard plots (Kapuscinski & Skoczylas, 1978) that were interpreted in terms of two binding sites, both with very low saturation values. The sum of these saturation values (0.036) is very close to the saturation value we obtained for site 1. We therefore propose that these sites are not unique but correspond to the first site that we observed with CD. AT preferentiality within this site is in fact expected to give a curved fluorescence Scatchard plot, owing to the higher fluorescence quantum yield in AT-rich regions (Cavatorta et al., 1985).

Absorbance and Linear Dichroism. From the knowledge of the amounts of DAPI bound in the two sites, site-specific spectra of absorption and linear dichroism can be calculated. Generally, from two absorption spectra recorded at different binding ratios, and the relative amounts known of the two species, a pair of equations can be solved:

$$A(r_1,\lambda) = f(r_1)A_1(\lambda) + [1 - f(r_1)]A_2(\lambda) \qquad (16)$$

$$A(r_2,\lambda) = f(r_2)A_2(\lambda) + [1 - f(r_2)]A_2(\lambda)$$

where $A(r_i,\lambda)$ is the absorption at ratio r_i and $A_1(\lambda)$ and $A_2(\lambda)$ are the respective site-specific spectra. In an analogous way the linear dichroism spectra can be obtained. The two site-specific absorbance and linear dichroism spectra and the corresponding LD^r spectra are shown in Figure 9. All spectra are normalized to unit concentration and the LD spectra to perfect flow orientation, with LD^r of the DNA bases used as a reference (Matsuoka & Nordén, 1982, 1983). It is seen that the extinction coefficient in site 2 is significantly lower than that in site 1, although the spectra are almost identical in shape. The maximum extinction coefficients of the resolved absorption spectra are given in Table I.

The linear dichroism spectra are somewhat different for the two species. The LD^r for the two transitions, estimated from the extreme values at short and long wavelengths, and calculated apparent angles (eq 3) are given in Table I. At higher binding ratios ($r > 0.05$) a small negative LD component is observed at wavelengths above 400 nm (results not shown). This effect can be ascribed to the previously considered exciton interaction of accidental dimers.

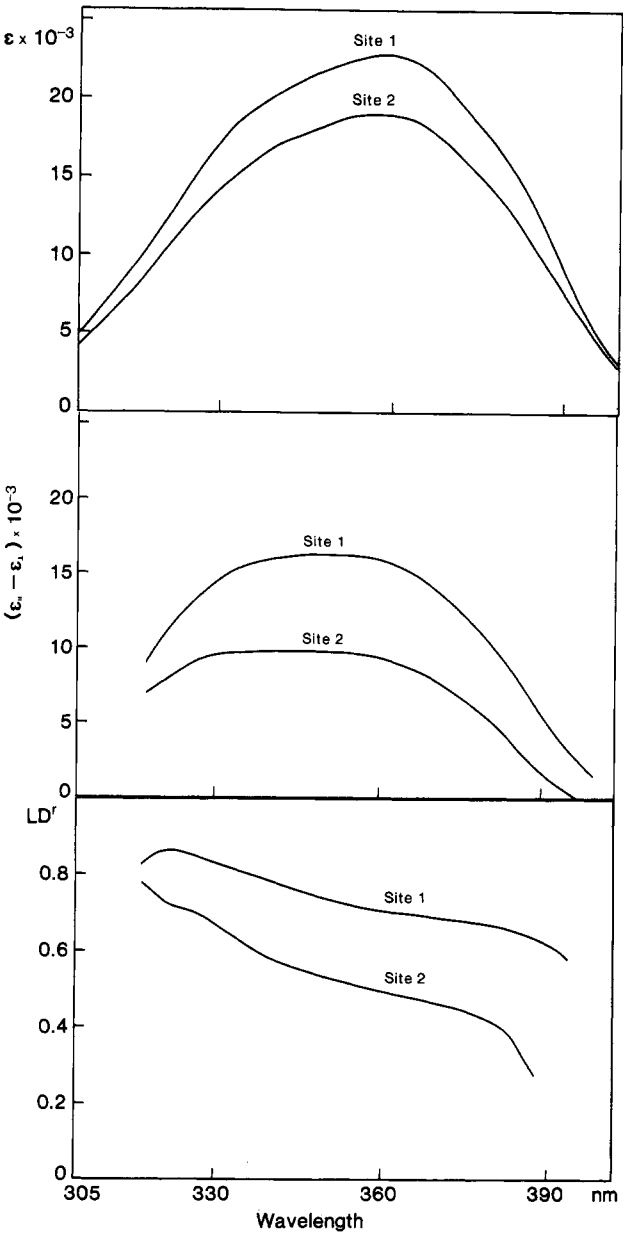

FIGURE 9: Site-specific absorbance (top), linear dichroism (middle), and reduced linear dichroism (bottom) spectra.

CD Mechanism. DAPI is not an optically active molecule but acquires CD when it binds to DNA. This can be due either to a chiral deformation of the DAPI molecule upon binding or to some chiral electronic interaction in its binding site. We cannot on the basis of our results discriminate between these alternatives, but a recent theoretical calculation indicates that DAPI should be planar when bound to DNA (Gresh, 1985). Still one must recall that also a weak, preferred chiral conformation might give a relatively strong intrinsic optical activity: for a long-axis polarized transition skewed into a

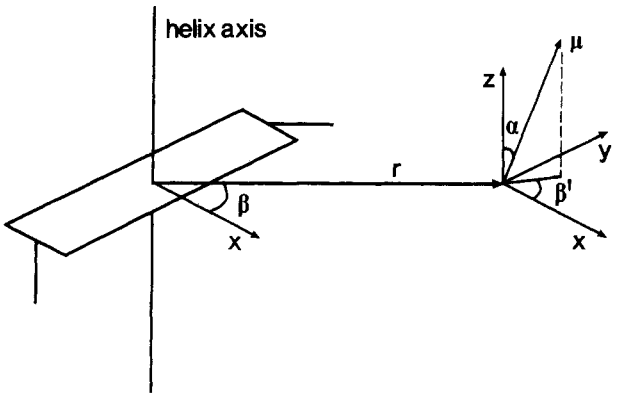

FIGURE 10: Definition of geometry used for calculation of induced CD. A right-handed coordinate system is chosen with the x axis as the bisector of the two glucosidic bonds, the z axis is parallel to the helix axis, r is the DAPI–DNA displacement vector, α is the angle between the transition moment in DAPI (μ) and the z axis, β is the angle between r and the x axis, and β' is the "azimuthal angle" of μ in the xy plane.

right-handed helix a positive CD will appear, and vice versa. We shall assume that the major contribution to CD is through interaction with the electric-dipole allowed $\pi \rightarrow \pi^*$ transitions of the chirally disposed DNA bases (neglecting any $n \rightarrow \pi^*$ transitions). For each pair of interacting (nondegenerate) transition moments, the contribution of rotational strength is calculated (Charney, 1979):

$$R_{DAPI} = -\frac{\nu_{DAPI}\nu_{DNA}}{c\hbar(\nu_{DNA}^2 - \nu_{DAPI}^2)} V(\mu_{DAPI},\mu_{DNA})(\mu_{DAPI} \times \mu_{DNA})\cdot\mathbf{r} \quad (17)$$

where μ_{DAPI} and μ_{DNA} are the transition moments of DAPI and DNA at frequencies ν_{DAPI} and ν_{DNA}, respectively, and V is the interaction energy which will be approximated as (dipole–dipole interaction)

$$V = (\mu_{DAPI}\cdot\mu_{DNA})/r^3 - 3[(\mu_{DAPI}\cdot\mathbf{r})(\mu_{DNA}\cdot\mathbf{r})/r^5] \quad (18)$$

The location of an adduct molecule (or rather its transition moment) can be defined relative to a DNA base pair, with three angles and a displacement vector ($\mathbf{r}$), as shown in Figure 10. The x axis is chosen as the bisector of the two glucosidic bonds in the direction of the minor groove, β is the angle between r and the x axis, α is the angle between the transition moment and the helix axis, and β' is the azimuthal angle defined by the projection of μ_{DAPI} in the xy plane.

Figure 11 shows the sign of the rotational strength calculated for varying β and β' angles, assuming a fixed $\alpha = 45°$ (which is the angle obtained from LD) and the DAPI transition moment at 335 nm at a distance of 7 Å to the center of the DNA axis. The transition moment directions and corresponding dipole strengths determined for the DNA bases in stretched films by Matsuoka and Nordén (1982, 1983) have been used. The contributions from up to 600 base pairs have been taken into account, and the fraction of 58% AT in calf thymus DNA has been used in the averaging procedure. Figure 11 can be used to eliminate certain binding geometries and will be exploited below to support a binding of DAPI in the grooves of DNA. A more detailed outline on sector rules for DNA adducts will be presented in a separate study.

Binding Geometry. Table I shows that the apparent angle between DAPI transition moments and the DNA helix axis, as obtained from LD, is close to 45° in both binding sites. It can be anticipated that DAPI remains essentially planar when bound to DNA (Gresh, 1985) and that the transition moments are restricted to the molecular plane ($\pi \rightarrow \pi^*$ transitions). The

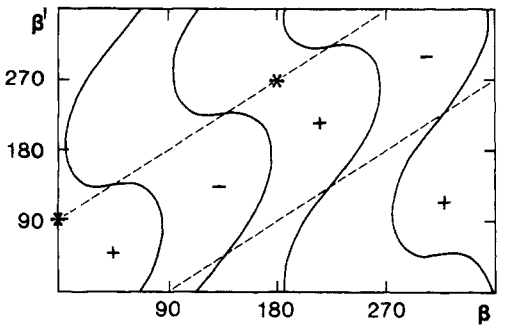

FIGURE 11: Sector rule for DNA-induced CD. Sign of rotational strength according to eq 18 as function of β and β' angles for the case $\alpha = 45°$ and a transition of 335 nm in a chromophore at a distance of 7 Å to the helix axis. Nodal lines are shown (—). Dashed lines show geometrical constraint between β and β' for a chromophore attached tangentially to the DNA helix axis. Positions in the middle of the grooves for a transition moment rising along the grooves are indicated by asterisks (*).

angle demonstrates that DAPI is strongly tilted in its DNA complex, a binding geometry that is incompatible with true intercalation.

In order to correlate the apparent angles in Table I with the orientation of the DAPI molecule relative to the DNA helix, we shall first consider the angles between the transition moments and the long axis of DAPI. If the molecular plane of DAPI is tilted toward the DNA helix, this angle will in part add to the apparent angle of 45°. The small wavelength dependence in the visible region of the LD^r spectrum (Figure 3) may indicate that the plane containing the two transition moments is indeed tilted in the complex. If the angle between the moments is small, this tilt could be quite large. LD measurements of DAPI in stretched films (B. Åkerman, M. Kubista, and B. Nordén, unpublished results) indicate that the angles between the two transition moments and the long axis of DAPI are less than 20°. Taking this into account, the angle between the long axis of DAPI and the helical axis will, in both sites, be about 45 ± 20° (with the maximum value corresponding to a 90° tilt). The minus sign seems not very likely, since it corresponds to a DAPI long-axis orientation almost parallel to the DNA axis. If we assume a moderate tilt, the angle will be some 50–60°, which is well in accord with the pitch angle between the grooves and the DNA axis (Bloomfield et al., 1974) at a distance of some 7 Å to the helix axis.

A binding of DAPI in the grooves of DNA is finally also supported from the sign and magnitude of the induced CD: a molecule tangentially attached to the DNA helix will have $\beta' = \beta + 90$, if the direction of the transition moment is parallel to the grooves of the helix, or $\beta' = \beta - 90$, if the direction is orthogonal to the grooves. These orientations are represented by the two lines in Figure 11. A molecule situated in the middle of a groove will be found at $\beta = 0°$ (minor groove) or $\beta = 180°$ (major groove). These locations for a transition moment directed along the grooves are denoted with stars in Figure 11 and both are found in regions predicted to give positive induced CD. The calculated rotational strength in both locations is 0.3 Debye–Bohr magneton (DBM), which result is in fair agreement with the rotational strength of 0.8 DBM obtained by integrating the CD envelope of the specific spectrum for DAPI in site 1 (Figure 7).

On the basis of the analogy with netropsin and on steric arguments, it has been speculated that site 1 is located in the minor groove of the DNA helix involving both hydrogen bonding and electrostatic interaction (Manzini et al., 1983). This hypothesis is supported by our results, and we suggest

that the first and second sites correspond to a binding of DAPI in the minor and major grooves, respectively. With a total saturation value of $n_1 + n_2 = 0.2$, not all DAPI molecules can be bound in the minor groove since each ligand will be covering at least 3 base pairs as judged from inspection of molecular models regarding the obtained binding angles. [That DAPI covers 3 base pairs has been observed by Manzini et al. (1983) from binding density considerations.] The slightly more pronounced wavelength dependence and lower magnitude of LD^r in site 2 compared to site 1 (Figure 9) can indicate that DAPI is more tilted or more mobile (Nordén, 1978) in this site. This could make hydrogen bonding between the indole nitrogen and the DNA bases less favorable and account for the higher sensitivity to ionic strength in site 2 (Manzini et al., 1983). Furthermore, the interior of the major groove is less negative (Pullman & Pullman, 1981), which could explain the weaker binding in this site.

Conclusions

Our results and arguments strongly support that DAPI has two binding sites on DNA. In both sites, the DAPI molecules display an acute tilt relative to the base planes and are bound in an nonintercalative way with their long axis approximately parallel to the grooves of the DNA helix. Binding geometries and site densities are consistent with a location of DAPI in the grooves, with the high-affinity site most probably in the minor groove. The binding, at least in the high-affinity site, is pereferential to AT-rich regions. At higher binding ratios, evidence is obtained for interactions between DAPI molecules in accidental proximity to each other, bound in the two sites.

Registry No. DAPI, 75980-76-6.

References

Arnott, S., Dover, S. D., & Wonacott, A. J. (1969) *Acta Crystallogr., Sect. B: Struct. Crystallogr. Cryst. Chem. 25B*, 2192–2206.

Bloomfield, V. A., Crothers, D. M., & Tinoco, I. (1974) *Physical Chemistry of Nucleic Acids*, Chapter 4, pp 104–130, Harper & Row, New York.

Bonnett, D., Heusêle, C., Simon, C., & Pantaloni, D. (1985) *J. Biol. Chem. 260*, 2819–2825.

Cantor, C. R., & Schimmel, P. R. (1980) *Biophysical Chemistry Part II: Techniques for the Study of Biological Structure and Function*, Chapter 8, pp 409–425, W. H. Freeman, San Francisco, CA.

Cavatorta, P., Masotti, L., & Szabo, A. G. (1985) *Biophys. Chem. 22*, 11–16.

Chandra, P., & Mildner, B. (1979) *Cell. Mol. Biol. 25*, 137–146.

Charney, E. (1979) *The Molecular Basis of Optical Activity*, Wiley, New York.

Coleman, A. W., Maguire, M. J., & Coleman, J. R. (1981) *J. Histochem. Cytochem. 29*, 959–968.

Dann, O., Bergen, G., Demant, E., & Volz, G. (1971) *Justus Liebigs Ann. Chem. 749*, 68–89.

Dattagupta, N., Hogan, M., & Crothers, D. M. (1980) *Biochemistry 19*, 5998–6005.

Davidsson, Å., & Nordén, B. (1976) *Chem. Scr. 9*, 49–53.

Ford, T. C., & Rickwood, D. (1984) *Nucleic Acids Res. 12*, 1219–1226.

Gardner, B. J., & Mason, S. F. (1967) *Biopolymers 5*, 79–94.

Gresh, N. (1985) *Int. J. Biol. Macromol. 7*, 199–202.

Kania, J., & Fanning, T. G. (1976) *Eur. J. Biochem. 67*, 367–371.

Kapuscinski, J., & Skoczylas, B. (1977) *Anal. Biochem. 83*, 252–257.

Kapuscinski, J., & Skoczylas, B. (1978) *Nucleic Acids Res. 5*, 3775–3799.

Kapuscinski, J., & Szer, W. (1979) *Nucleic Acids Res. 6*, 3519–3534.

Kapuscinski, J., & Yanagi, K. (1979) *Nucleic Acids Res. 6*, 3535–3542.

Langlois, R. G., Carrano, A. V., Stay, J. W., & Van Dilla, M. A. (1980) *Chromosoma 77*, 229–251.

Lee, G. M., Thornthwaite, J. T., & Rasch, E. M. (1984) *Anal. Biochem. 137*, 221–226.

Lin, M. S., Comings, D. E., & Alfi, O. S. (1977) *Chromosoma 60*, 15–25.

Mahler, H. R., Kline, B., & Mehrota, B. D. (1964) *J. Mol. Biol. 9*, 801–811.

Manzini, G., Barcellona, M. L., Avitabile, M., & Quadrifoglio, F. (1983) *Nucleic Acids Res. 11*, 8861–8876.

Masotti, L., Cavatorta, P., Avitabile, M., Barcellona, M. L., von Berger, J., & Ragusa, N. (1982) *Ital. J. Biochem. 31*, 90–99.

Matsuoka, Y., & Nordén, B. (1982) *Biopolymers 21*, 2433–2452.

Matsuoka, Y., & Nordén, B. (1983) *Biopolymers 22*, 1731–1746.

Mazus, B., Falchuk, K. H., & Vallee, B. L. (1986) *Biochemistry 25*, 2941–2945.

Müller, W., & Gautier, F. (1975) *Eur. J. Biochem. 54*, 385–394.

Naimski, P., Bierzynski, A., & Fikus, M. (1980) *Anal. Biochem. 106*, 471–475.

Nordén, B. (1978) *Appl. Spectrosc. Rev. 14*, 157–248.

Nordén, B., & Tjerneld, F. (1976) *Biophys. Chem. 4*, 191–198.

Nordén, B., & Tjerneld, F. (1982) *Biopolymers 21*, 1713–1734.

Nordén, B., & Seth, S. (1985) *Appl. Spectrosc. 39*, 647–655.

Patel, D. J. (1982) *Proc. Natl. Acad. Sci. U.S.A. 79*, 6424–6428.

Pullman, A., & Pullman, B. (1981) *Q. Rev. Biophys. 14*, 289–380.

Schweizer, D. (1976) *Exp. Cell Res. 102*, 408–409.

Stepien, E., Filutowicz, M., & Fikus, M. (1979) *Acta Biochim. Pol. 26*, 29–38.

Tijssen, J. P. F., Beekes, H. W., & van Steveninck, J. (1982) *Biochim. Biophys. Acta 721*, 394–398.

Wada, A., & Kozawa, S. (1964) *J. Polym. Sci., Part A 2*, 853–864.

Waring, M. (1970) *J. Mol. Biol. 54*, 247–279.

Williamson, D. H., & Fennel, D. J. (1975) *Methods Cell Biol. 12*, 335–351.